

A Class of Axis–Angle Attitude Control Laws for Rotational Systems

Francisco M. F. R. Gonçalves, *Graduate Student Member, IEEE*, Ryan M. Bena, *Member, IEEE*, and Néstor O. Pérez-Arancibia, *Member, IEEE*

Abstract—We introduce a new class of attitude control laws for rotational systems; the proposed framework generalizes the use of the Euler axis–angle representation beyond quaternion-based formulations. Using basic Lyapunov stability theory and the notion of extended class \mathcal{K} function, we developed a method for determining and enforcing the global asymptotic stability of the single fixed point of the resulting *closed-loop* (CL) scheme. In contrast with traditional quaternion-based methods, the introduced generalized axis–angle approach enables greater flexibility in the design of the control law, which is of great utility when employed in combination with a switching scheme whose transition state depends on the angular velocity of the controlled rotational system. Through simulation and real-time experimental results, we demonstrate the effectiveness of the developed formulation. According to the recorded data, in the execution of high-speed tumble-recovery maneuvers, the new method consistently achieves shorter stabilization times and requires lower control effort relative to those corresponding to the quaternion-based and geometric-control methods used as benchmarks.

Index Terms—Axis–angle, attitude control, robotics.

I. INTRODUCTION

NUMEROUS different types of attitude controllers have been proposed for stabilizing and commanding the trajectory of rotational systems that can be modeled as rigid bodies [1]–[16]. These controllers can be classified into three main types: (i) quaternion-based, (ii) Euler-angles–based, and (iii) rotation-matrix–based (geometric). The limitations of attitude controllers based on Euler angles have been extensively studied and discussed in the technical literature—for example, see [17] and references therein. Due to these limitations, quaternion-based and geometric methods have been the preferred choices for representing and implementing robust high-performance attitude controllers. Although these two formulations implicitly contain the knowledge about the Euler axis and associated rotation angle as defined in [18], this information is generally not directly used in controller design.

This work was supported in part by the Washington State University (WSU) Foundation and the Palouse Club through a Cougar Cage Award to N. O. Pérez-Arancibia and in part by the WSU Voiland College of Engineering and Architecture through a start-up package to N. O. Pérez-Arancibia.

F. M. F. R. Gonçalves and R. M. Bena contributed equally to this work. F. M. F. R. Gonçalves and N. O. Pérez-Arancibia are with the School of Mechanical and Materials Engineering, Washington State University (WSU), Pullman, WA 99164-2920, USA. R. M. Bena is with the Department of Mechanical and Civil Engineering, California Institute of Technology, Pasadena, CA 91125-2100, USA. Corresponding authors' email: francisco.goncalves@wsu.edu (F. M. F. R. G.); n.perezarancibia@wsu.edu (N. O. P.-A.).

For example, quaternion-based time-invariant attitude control laws usually include a proportional term that is formed by scaling the attitude-error Euler axis with $\sin \frac{\Theta_e}{2}$, where Θ_e is the corresponding instantaneous rotation error. However, there is no reason for this type of formulation other than ensuring continuity in the entire rotational space and simplifying the analysis of the resulting *closed-loop* (CL) system. Counterintuitively, however, in most practical applications, this continuous formulation is modified to obtain a switching or hybrid scheme in order to avoid unwinding behavior [4]–[8]. Another characteristic of continuous quaternion-based control laws is that, for rotational errors larger than π rad, the proportional control effort decreases as the rotational error about the attitude-error Euler axis increases. Also, it can be shown that geometric-based attitude control laws implicitly apply torques in the direction of the shorter rotational trajectory required to eliminate the attitude error. As discussed in [1] and [2], this direction choice is not necessarily the best for every kinematic situation, depending on the specific performance objectives of the problem of interest.

In this letter, we introduce a class of attitude control laws applicable to a wide gamut of rigid rotational systems moving in the *three-dimensional* (3D) space, including *uncrewed aerial vehicles* (UAVs), satellites, and microbotic swimmers. The proposed method generalizes the use of the Euler axis–angle representation in the formulation of the feedback law that stabilizes and drives the rotational motion of the controlled system. It is well known that global asymptotic stability on the special orthogonal group in three dimensions, $SO(3)$, cannot be achieved with the use of continuous time-invariant feedback controllers. A common technique used to overcome this topological obstruction is to design discontinuous control laws [8]; another option is to define the CL dynamics of the controlled system on a covering that generates a unique coordinate representation of $SO(3)$, rather than on $SO(3)$ itself. Following this latter approach, by combining Lyapunov stability theory and the notion of extended class \mathcal{K} function, we developed a method that ensures the existence of a unique CL fixed *attitude-error quaternion* (AEQ) and the global asymptotic stability of the corresponding equilibrium point, which depends on positive-definiteness conditions that the controller gains must satisfy.

A main contribution of the work presented in this letter is the design flexibility enabled by a generalized formulation of the proportional term in the proposed control law; specifically, it allows the user to select a suitable proportional control function based on the platform and/or application, with stability guarantees. Furthermore, in contrast to existing quaternion-based control methods, the new generalized axis–angle attitude control approach ensures a greater propor-

tional action the farther the system's state is from the stable CL fixed AEQ. This characteristic is especially useful when a scheme of the proposed type is employed in combination with intelligent switching methods capable of taking into account the angular velocity when selecting the direction in which the proportional component of the input torque is applied during operation, as for example done in the case presented in [1]. We tested the functionality and performance of the introduced approach through simulations and outdoor flight tests. The obtained simulation and experimental data show that, compared to two other high-performance benchmark controllers—one quaternion-based and another geometric—a scheme of the new type is unequivocally superior. Specifically, measurements obtained through dozens of high-speed tumble-recovery maneuvers show that the presented approach consistently achieves shorter stabilization times and requires less control effort, from a statistical standpoint.

Notation—

- 1) Lowercase symbols represent scalars, e.g., p ; bold lowercase symbols denote vectors, e.g., \mathbf{p} ; bold uppercase symbols denote matrices, e.g., \mathbf{P} ; and, bold crossed lowercase symbols denote quaternions, e.g., \mathbf{p} .
- 2) The set of unit 3D vectors is denoted by \mathcal{S}^2 .
- 3) The sets of reals and positive reals are denoted by \mathbb{R} and $\mathbb{R}_{>0}$, respectively. The set of integers is denoted by \mathbb{Z} .
- 4) The symbols \times and \otimes denote the cross-product of two vectors and multiplication between two quaternions, respectively.
- 5) Throughout the rest of the paper, we use the notion of extended class \mathcal{K} function as defined in [19].

II. BACKGROUND

We first describe the dynamics of a rigid body rotating in the 3D space. As shown in Fig. 1, $\mathcal{B} = \{\mathbf{b}_1, \mathbf{b}_2, \mathbf{b}_3\}$ denotes the body-fixed frame of reference, with its origin coinciding with the body's *center of mass* (CoM), used for kinematic description and dynamic analysis. Consistent with this definition, $\mathcal{I} = \{\mathbf{i}_1, \mathbf{i}_2, \mathbf{i}_3\}$ denotes the chosen inertial frame of reference fixed to the planet. As discussed in [4] and [5], using quaternions and Euler's second law, the open-loop rotational dynamics of the system can be described as

$$\dot{\mathbf{q}} = \frac{1}{2} \mathbf{q} \otimes \begin{bmatrix} 0 \\ \boldsymbol{\omega} \end{bmatrix}, \quad (1a)$$

$$\dot{\boldsymbol{\omega}} = \mathbf{J}^{-1} (\boldsymbol{\tau} - \boldsymbol{\omega} \times \mathbf{J} \boldsymbol{\omega}), \quad (1b)$$

in which \mathbf{q} is a unit quaternion that represents the orientation of \mathcal{B} relative to \mathcal{I} ; $\boldsymbol{\omega}$ is the angular velocity of \mathcal{B} with respect to \mathcal{I} , written in \mathcal{B} coordinates; \mathbf{J} is the inertia matrix of the body, written in \mathcal{B} coordinates; and, $\boldsymbol{\tau}$ is the torque applied to the system written in \mathcal{B} coordinates and, in closed loop, generated by a control law.

As specified by Euler's rotation theorem, any sequence of rotations of a rigid body in the 3D space is equivalent to a single rotation of amount Θ about an axis \mathbf{u} that passes through the body's CoM. This information can be stored in the form of a unit quaternion as $\mathbf{q} = [m \mathbf{n}^T]^T$, where $m = \cos \frac{\Theta}{2}$ and $\mathbf{n} = \mathbf{u} \sin \frac{\Theta}{2}$. In the case specified by (1a), Θ is the amount that the modeled body must be rotated about \mathbf{u} to reach the attitude of \mathcal{B} starting from that of \mathcal{I} . Accordingly, the instantaneous



Fig. 1. **Flight control tests and frames of reference.** This picture shows the UAV, a Crazyflie 2.1, used in the control experiments, and the inertial and body-fixed frames of reference, $\mathcal{I} = \{\mathbf{i}_1, \mathbf{i}_2, \mathbf{i}_3\}$ and $\mathcal{B} = \{\mathbf{b}_1, \mathbf{b}_2, \mathbf{b}_3\}$. Here, \mathcal{B} , whose origin coincides with the robot's CoM, is shown shifted for clarity.

AEQ is given by $\mathbf{q}_e = \mathbf{q}^{-1} \otimes \mathbf{q}_d = [m_e \mathbf{n}_e^T]^T$, with $m_e = \cos \frac{\Theta_e}{2}$ and $\mathbf{n}_e = \mathbf{u}_e \sin \frac{\Theta_e}{2}$, where Θ_e is the amount that \mathcal{B} must be rotated about the attitude-error Euler axis, \mathbf{u}_e , to reach the orientation of the desired body-fixed frame, \mathcal{B}_d ; and, \mathbf{q}_d is a unit quaternion that represents the attitude of \mathcal{B}_d relative to \mathcal{I} . In practice, \mathbf{q}_d is either defined by the user, as described in Section IV, or generated by a position control scheme, as explained in [4]. Any real-time control algorithm based on the formulation specified by (1b) requires the desired angular velocity of the controlled rotational system in \mathcal{B} coordinates, $\boldsymbol{\omega}_d$. To compute this variable, we first obtain the corresponding desired angular-velocity quaternion, written in \mathcal{B}_d coordinates, according to

$$\begin{bmatrix} 0 \\ \hat{\boldsymbol{\omega}}_d \end{bmatrix} = 2\mathbf{q}_d^{-1} \otimes \dot{\mathbf{q}}_d. \quad (2)$$

Then, we compute $\boldsymbol{\omega}_d = \mathbf{S}^T \mathbf{S}_d \hat{\boldsymbol{\omega}}_d$, where \mathbf{S}_d transforms vectors from \mathcal{B}_d to \mathcal{I} coordinates, and \mathbf{S}^T transforms vectors from \mathcal{I} to \mathcal{B} coordinates. Thus, using these kinematic variables, we can define a control law that computes the torque input as

$$\boldsymbol{\tau}_b = \mathbf{J} (k_q \mathbf{n}_e + k_\omega \boldsymbol{\omega}_e + \dot{\boldsymbol{\omega}}_d) + \boldsymbol{\omega} \times \mathbf{J} \boldsymbol{\omega}, \quad (3)$$

where k_q and k_ω are scalar positive real controller gains; $\boldsymbol{\omega}_e = \boldsymbol{\omega}_d - \boldsymbol{\omega}$ is the angular-velocity tracking error; $\mathbf{J} \dot{\boldsymbol{\omega}}_d$ is a feedforward term that approximately cancels the left-hand side of (1b) and is included with the objective of providing faster tracking performance; and, $\boldsymbol{\omega} \times \mathbf{J} \boldsymbol{\omega}$ is a feedback-linearization term that cancels the nonlinearity present in (1b).

As discussed in [4], the CL rotational dynamics obtained by substituting the right-hand side of (3) into (1b) exhibit two equilibria corresponding to the same kinematic condition but with different stability properties—one asymptotically stable and the other unstable. It is straightforward to see that, at both fixed points, $\mathbf{n}_e = \mathbf{0}$. Therefore, if the state of the CL system were to be exactly at the unstable equilibrium, the control torque specified by (3) would not compel the controlled rotational system to execute a 2π -rad rotation and converge to the stable equilibrium, thus preventing global asymptotic stability on $\mathcal{SO}(3)$. However, in any real-world application, any deviation from the unstable fixed point would make $\mathbf{n}_e \neq \mathbf{0}$ and, therefore, for all practical purposes, we can confidently assume that the torque generated according to (3) forces the CL system's state to converge to the stable equilibrium. Additionally, note that since \mathbf{n}_e is scaled by the factor $\sin \frac{\Theta_e}{2}$, the first term in (3) does not provide the maximum allowable control effort when

the controlled rotational system is at the farthest orientation from the stable CL equilibrium AEQ. In fact, this term reaches its minimum value at the unstable CL fixed AEQ, where $\Theta_e = 2\pi$ rad; its maximum at $\Theta_e = \pi$ rad; and, its minimum again at the stable CL equilibrium AEQ, where $\Theta_e = 0$ rad. These observations contradict the expected behavior of the proportional action of a feedback controller. We address these representational, stability, and performance issues in the next section by proposing a new generalized axis-angle attitude law for controlling rotational systems in the 3D space.

III. GENERALIZED AXIS-ANGLE ATTITUDE CONTROL

A. A New Class of Control Laws

Let $\gamma: \mathbb{R} \mapsto \mathbb{R}$ be an extended class \mathcal{K} function. Then, for a system whose dynamics evolve on $\mathbf{SO}(3)$, the rotational errors to be minimized can be represented as

$$\alpha_e = \gamma(\Theta_e)\mathbf{u}_e \quad \text{and} \quad \omega_e, \quad (4)$$

where α_e is a *scaled Euler axis* (SEA) aligned with \mathbf{u}_e , whose magnitude—measured by any vector norm—scales with the value of Θ_e . Without loss of coverage of $\mathbf{SO}(3)$, Θ_e can be restricted to any half-open interval spanning 2π that includes 0; in this letter, we consider $\Theta_e \in [0, 2\pi)$. Consistent with this selection, for any $\Theta_e \neq 0$, an axis-angle pair, $\{\mathbf{u}_e, \Theta_e\}$, uniquely defines one of the two possible rotations—with opposite directions—that would cancel the instantaneous attitude error of the controlled rotational system. When $\Theta_e = 0$, the corresponding rotation axis is not uniquely defined and can take any value in \mathcal{S}^2 ; however, α_e is still well defined. To initialize simulations and experiments, we select the direction of rotation at initial time t_0 that minimizes, assuming $\Theta_e \in [0, 2\pi)$, a two-valued cost function, as described in [1]. Thus, using the errors specified by (4), we define the proposed generic control law as

$$\boldsymbol{\tau}_\gamma = \mathbf{J}(k_\alpha \alpha_e + k_\delta \dot{\alpha}_e + k_\omega \omega_e + \dot{\omega}_d) + \boldsymbol{\omega} \times \mathbf{J}\boldsymbol{\omega}, \quad (5)$$

in which k_α , k_δ , and $k_\omega \in \mathbb{R}_{>0}$. Then, from simple substitution of (4) into (5), we obtain that

$$\boldsymbol{\tau}_\gamma = \mathbf{J} [k_\alpha \gamma(\Theta_e)\mathbf{u}_e + k_\delta \gamma(\Theta_e)\dot{\mathbf{u}}_e + k_\delta \dot{\gamma}(\Theta_e)\mathbf{u}_e + k_\omega \omega_e + \dot{\omega}_d] + \boldsymbol{\omega} \times \mathbf{J}\boldsymbol{\omega}. \quad (6)$$

B. Closed-Loop Dynamics and Equilibrium Points

It is straightforward to see that for the control input defined by (6), the CL rotational-error dynamics can be written as

$$\dot{\mathbf{q}}_e = \frac{1}{2} \begin{bmatrix} 0 \\ \boldsymbol{\omega}_e \end{bmatrix} \otimes \mathbf{q}_e, \quad (7a)$$

$$\dot{\boldsymbol{\omega}}_e = -k_\alpha \gamma(\Theta_e)\mathbf{u}_e - k_\delta \left[\gamma(\Theta_e)\dot{\mathbf{u}}_e + \frac{d\gamma}{d\Theta_e}(\mathbf{u}_e^T \boldsymbol{\omega}_e)\mathbf{u}_e \right] - k_\omega \boldsymbol{\omega}_e, \quad (7b)$$

in whose derivation we used that $\dot{\Theta}_e = \mathbf{u}_e^T \boldsymbol{\omega}_e$. Next, to find the equilibrium point(s) of the system given by (7a)–(7b), we solve the set of algebraic equations specified by

$$-\frac{1}{2} \mathbf{n}_e^T \boldsymbol{\omega}_e = 0, \quad (8a)$$

$$-\frac{1}{2} (\mathbf{n}_e \times \boldsymbol{\omega}_e - m_e \boldsymbol{\omega}_e) = \mathbf{0}_{3 \times 1}, \quad (8b)$$

$$-k_\alpha \gamma(\Theta_e)\mathbf{u}_e - k_\delta \gamma(\Theta_e)\dot{\mathbf{u}}_e - k_\omega \boldsymbol{\omega}_e = \mathbf{0}_{3 \times 1}. \quad (8c)$$

For (8b) to be satisfied, both terms inside the parenthesis must be zero because they are orthogonal. For both these terms to be zero, one of the following statements must hold: (i) $\mathbf{n}_e \parallel \boldsymbol{\omega}_e$ and $m_e = 0$; (ii) $\boldsymbol{\omega}_e = \mathbf{0}$; (iii) $\mathbf{n}_e = \boldsymbol{\omega}_e = \mathbf{0}$. Also, for (8a) to be satisfied, either (ii) or (iii) is true, $\mathbf{n}_e = \mathbf{0}$, or $\mathbf{n}_e \perp \boldsymbol{\omega}_e$. Since \mathbf{n}_e and $\boldsymbol{\omega}_e$ cannot simultaneously be orthogonal and parallel, the only viable option is either (ii) or (iii). The fulfillment of either (ii) or (iii) requires that the solution to (8a)–(8c) satisfies $\boldsymbol{\omega}_e^* = \mathbf{0}$. Since \mathbf{u}_e is a vector evolving on \mathcal{S}^2 , it follows that $\mathbf{u}_e \perp \dot{\mathbf{u}}_e$ and, therefore, for (8c) to be satisfied, $\gamma(\Theta_e) = 0$. Last, recalling that $\gamma(\Theta_e)$ is an extended class \mathcal{K} function and, therefore, $\gamma(0) = 0$, we conclude that $\Theta_e^* = 0$.

For the law specified by (6), we selected $\gamma(\Theta_e)$ to be an extended class \mathcal{K} function in order to enforce the existence of a unique zero for $\gamma(\Theta_e)$ and a unique equilibrium point for the CL dynamics given by (7a)–(7b), over the selected range of Θ_e . In summary, the CL dynamics resulting from using the control input specified by (6) exhibit a unique equilibrium, given by the quaternion-vector pair $\mathbf{q}_e^* = [1 \ 0 \ 0 \ 0]^T$ and $\boldsymbol{\omega}_e^* = \mathbf{0}$, for $\Theta_e \in [0, 2\pi)$. This result does not contradict the topological obstruction discussed in [17]—according to which all continuous time-invariant CL vector fields on $\mathbf{SO}(3)$ must exhibit multiple equilibria—as the CL dynamics are defined on an axis-angle covering that generates a unique coordinate representation of each rotation in $\mathbf{SO}(3)$, rather than on $\mathbf{SO}(3)$ itself. Furthermore, for $\Theta_e \in (-\infty, \infty)$, the term $\gamma(\Theta_e)\mathbf{u}_e$ is discontinuous at $\Theta_e = 2\pi k$ rad, for all nonzero $k \in \mathbb{Z}$. As a result, the CL dynamics specified by (7a)–(7b) are also discontinuous, which forces the existence of a unique fixed point, similarly to the cases presented in [8]. However, discontinuities produce numerous experimental and theoretical problems; for example, to analyze the differential equations of the CL system specified by (7a)–(7b) when $\Theta_e \in (-\infty, \infty)$, we must use Carathéodory's notion of solution, as stated in [20, Definition 2.1]. For these reasons, $\Theta_e \in [0, 2\pi)$ is a superior choice for the problem considered in this letter.

C. Stability Analysis

Theorem 1. Let the attitude and angular-velocity references, \mathbf{q}_d and $\boldsymbol{\omega}_d$, be smooth and bounded functions of time. Also, let the real controller gains satisfy $k_\delta > 0$, $k_\omega > 0$, and $k_\alpha > \frac{k_\delta k_\omega}{4}$. Then, the fixed point $\{\Theta_e^*, \boldsymbol{\omega}_e^*\}$ of the CL state-space rotational dynamics specified by (7a) and (7b) is globally asymptotically stable on the domain $\mathcal{D} = \{ \{\Theta_e, \boldsymbol{\omega}_e\} \mid \Theta_e \in [0, 2\pi), \boldsymbol{\omega}_e \in \mathbb{R}^3 \}$, for any initial state $\{\Theta_e(t_0), \boldsymbol{\omega}_e(t_0)\} \in \mathcal{D}$ and $\mathbf{u}_e(t_0) \in \mathcal{S}^2$.

Proof. Let a candidate Lyapunov function be

$$V = \begin{bmatrix} \gamma(\Theta_e)\mathbf{u}_e^T & \boldsymbol{\omega}_e^T \end{bmatrix} \begin{bmatrix} \frac{k_\delta^2}{2k_\alpha} & \frac{k_\delta}{2k_\alpha} \\ \frac{k_\delta}{2k_\alpha} & 1 \end{bmatrix} \begin{bmatrix} \gamma(\Theta_e)\mathbf{u}_e \\ \boldsymbol{\omega}_e \end{bmatrix} + \int_0^{\Theta_e} \gamma(\phi) d\phi, \quad (9)$$

for $\Theta_e \in [0, 2\pi)$. It is straightforward to show that the eigenvalues of the matrix in the quadratic term of (9) are

$$\lambda_1 = 0 \quad \text{and} \quad \lambda_2 = \frac{k_\delta^2 + 1}{2k_\alpha}. \quad (10)$$

Therefore, the quadratic term in (9) is positive semidefinite and V is positive definite because the integral term is positive definite with respect to $\Theta_e \in [0, 2\pi)$, for any extended class \mathcal{K} function γ . To continue, we expand V as

$$V = \frac{k_\delta^2}{2k_\alpha} \gamma^2(\Theta_e) + \frac{k_\delta}{k_\alpha} \gamma(\Theta_e) \mathbf{u}_e^T \boldsymbol{\omega}_e + \frac{1}{2k_\alpha} \boldsymbol{\omega}_e^T \boldsymbol{\omega}_e + \int_0^{\Theta_e} \gamma(\phi) d\phi, \quad (11)$$

and compute its time derivative, which yields

$$\begin{aligned} \dot{V} &= \frac{k_\delta^2}{k_\alpha} \gamma(\Theta_e) \frac{d\gamma}{d\Theta_e} \dot{\Theta}_e \\ &+ \frac{k_\delta}{k_\alpha} \left[\frac{d\gamma}{d\Theta_e} \dot{\Theta}_e \mathbf{u}_e^T \boldsymbol{\omega}_e + \gamma(\Theta_e) \dot{\mathbf{u}}_e^T \boldsymbol{\omega}_e + \gamma(\Theta_e) \mathbf{u}_e^T \dot{\boldsymbol{\omega}}_e \right] \\ &+ \frac{1}{k_\alpha} \boldsymbol{\omega}_e^T \dot{\boldsymbol{\omega}}_e + \gamma(\Theta_e) \dot{\Theta}_e. \end{aligned} \quad (12)$$

This expression can be simplified by recalling that $\dot{\Theta}_e = \mathbf{u}_e^T \boldsymbol{\omega}_e$, noticing that $\dot{\mathbf{u}}_e^T \boldsymbol{\omega}_e = 0$ because $\mathbf{u}_e \in \mathcal{S}^2$, and substituting (7b) into (12). Namely,

$$\begin{aligned} \dot{V} &= \frac{k_\delta^2}{k_\alpha} \gamma(\Theta_e) \frac{d\gamma}{d\Theta_e} \mathbf{u}_e^T \boldsymbol{\omega}_e \\ &+ \frac{k_\delta}{k_\alpha} \left[\frac{d\gamma}{d\Theta_e} \mathbf{u}_e^T \boldsymbol{\omega}_e \mathbf{u}_e^T \boldsymbol{\omega}_e + \gamma(\Theta_e) \dot{\mathbf{u}}_e^T \boldsymbol{\omega}_e - k_\alpha \gamma^2(\Theta_e) \right. \\ &\quad \left. - k_\delta \gamma(\Theta_e) \frac{d\gamma}{d\Theta_e} (\mathbf{u}_e^T \boldsymbol{\omega}_e) - k_\omega \gamma(\Theta_e) \mathbf{u}_e^T \boldsymbol{\omega}_e \right] \\ &+ \frac{1}{k_\alpha} \boldsymbol{\omega}_e^T \left[-k_\alpha \gamma(\Theta_e) \mathbf{u}_e - k_\delta \left(\gamma(\Theta_e) \dot{\mathbf{u}}_e \right. \right. \\ &\quad \left. \left. + \frac{d\gamma}{d\Theta_e} (\mathbf{u}_e^T \boldsymbol{\omega}_e) \mathbf{u}_e \right) - k_\omega \boldsymbol{\omega}_e \right] + \gamma(\Theta_e) \mathbf{u}_e^T \boldsymbol{\omega}_e. \end{aligned} \quad (13)$$

Thus, after canceling out the terms with equal magnitudes and opposite signs, we obtain

$$\begin{aligned} \dot{V} &= -k_\delta \gamma^2(\Theta_e) - \frac{k_\delta k_\omega}{k_\alpha} \gamma(\Theta_e) \mathbf{u}_e^T \boldsymbol{\omega}_e - \frac{k_\omega}{k_\alpha} \boldsymbol{\omega}_e^T \boldsymbol{\omega}_e \\ &= - \left[\gamma(\Theta_e) \mathbf{u}_e^T \quad \boldsymbol{\omega}_e^T \right] \mathbf{W} \begin{bmatrix} \gamma(\Theta_e) \mathbf{u}_e \\ \boldsymbol{\omega}_e \end{bmatrix}, \end{aligned} \quad (14)$$

where

$$\mathbf{W} = \begin{bmatrix} k_\delta & \frac{k_\delta k_\omega}{2k_\alpha} \\ \frac{k_\delta k_\omega}{2k_\alpha} & \frac{k_\omega}{k_\alpha} \end{bmatrix}, \quad (15)$$

which can be made positive definite by selecting

$$\{k_\delta, k_\omega\} > 0 \quad \text{and} \quad k_\alpha > \frac{k_\delta k_\omega}{4}, \quad (16)$$

thus also enforcing that $\dot{V}(\Theta_e, \boldsymbol{\omega}_e) < 0$ for all $\{\Theta_e, \boldsymbol{\omega}_e\} \neq \{\Theta_e^*, \boldsymbol{\omega}_e^*\}$, and $\dot{V}(\Theta_e^*, \boldsymbol{\omega}_e^*) = 0$. In summary, V is positive definite on \mathcal{D} and coercive in $\boldsymbol{\omega}_e$; therefore, proper on \mathcal{D} . Moreover, since \dot{V} is negative definite on \mathcal{D} , we conclude that the unique equilibrium of the CL dynamics given by (7a)–(7b) is globally asymptotically stable on \mathcal{D} , which, together with \mathcal{S}^2 , provides a complete covering of $\mathcal{SO}(3)$. \square

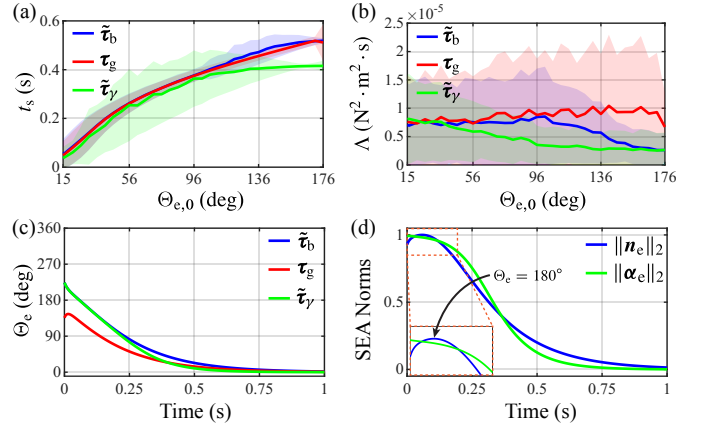


Fig. 2. Numerical results obtained with Crazyflie 2.1 parameters, using quaternion-based, geometric, and axis-angle control laws. (a) Mean and ESD of the stabilization time as functions of the initial rotation error. **(b)** Mean and ESD of the control effort as functions of the initial rotation error. **(c)** Time evolution of the rotation error associated with the attitude-error Euler axis. **(d)** Time evolution of the SEA magnitudes corresponding to the simulated quaternion-based and proposed axis-angle laws.

D. Discussion

There exist infinitely many valid choices of γ functions; some superior to the rest. For example, a sigmoid function is an extended class \mathcal{K} function that provides tunable saturation while maintaining linearity near the equilibrium. Namely,

$$\gamma(\Theta_e) = \Theta_{\max} \frac{1 - e^{-\xi \frac{\Theta_e}{\Theta_{\max}}}}{1 + e^{-\xi \frac{\Theta_e}{\Theta_{\max}}}}, \quad (17)$$

where Θ_{\max} and ξ are design parameters. In this context, Θ_{\max} is the angle at which the maximum magnitude of the actuation torque occurs and ξ determines the rate at which the magnitude of $\gamma(\Theta_e)$ changes with respect to Θ_e . Taking the derivative of (17) with respect to Θ_e yields

$$\frac{d\gamma}{d\Theta_e} = \frac{2\xi e^{-\xi \frac{\Theta_e}{\Theta_{\max}}}}{\left(1 + e^{-\xi \frac{\Theta_e}{\Theta_{\max}}}\right)^2}, \quad (18)$$

which provides insights and can be used to guide the process of controller synthesis. In particular, the slope at the origin has the form $\frac{d\gamma}{d\Theta_e}(0) = \frac{\xi}{2}$, where ξ can be tuned considering actuator limitations and control objectives.

IV. SIMULATION AND EXPERIMENTAL RESULTS

A. Numerical Simulations

To systematically assess the functionality and performance of the proposed generalized control law, we compared a controller synthesized using this new approach with two benchmark schemes through numerical simulations. The first scheme used for comparison uses the quaternion-based attitude control law specified by (3), τ_b ; the second is the high-performance geometric approach presented in [12], whose corresponding attitude control law here we denote by τ_g . We implemented and executed the numerical simulations in Simulink 25.2 (MATLAB R2025b), using the Dormand–Prince algorithm with a fixed time step of 10^{-4} s. The simulations were set up using the open-loop dynamical model speci-

fied by (1a)–(1b) with the parameters of the Crazyflie 2.1 platform—shown in Fig. 1—and controllers with empirically selected gains that satisfy the stability conditions for the three compared laws. Specifically, we used $\mathbf{J} = \text{diag}\{16.6, 16.7, 29.3\} \times 10^{-6} \text{ kg} \cdot \text{m}^2$, $k_q = 10^3 \text{ s}^{-2}$, and $k_\omega = 10^2 \text{ rad}^{-1} \cdot \text{s}^{-1}$ for τ_b specified by (3). For τ_γ specified by (5), we used the same \mathbf{J} and k_ω that for τ_b , and $k_\alpha = 10^3 \text{ rad}^{-1} \cdot \text{s}^{-2}$, $k_\delta = 10 \text{ rad}^{-1} \cdot \text{s}^{-1}$, and the function $\gamma(\Theta_e)$ defined by (17). For $\gamma(\Theta_e)$, we used $\Theta_{\max} = 1 \text{ rad}$ and $\xi = 1.5$, which were chosen considering the characteristics of the actuators driving the experimental platform. The controller gains for τ_g were specified to ensure a fair comparison. For consistency with previous published results, we implemented both τ_γ and τ_b in combination with the *model predictive selection* (MPS) algorithm presented in [1], according to which the instantaneous direction of \mathbf{u}_e , encoded by $\sigma \in \{-1, +1\}$, minimizes

$$\Gamma(\sigma, t) = \int_t^{t+t_h} [\boldsymbol{\tau}^T(\sigma, \zeta) \mathbf{R} \boldsymbol{\tau}(\sigma, \zeta) + \mathbf{n}_e^T(\zeta) \mathbf{Q} \mathbf{n}_e(\zeta)] d\zeta, \quad (19)$$

in which $t_h = 0.2 \text{ s}$; $\mathbf{R} = \mathbf{I}$, where \mathbf{I} is the identity matrix; and, $\mathbf{Q} = 10^{-6} \times \mathbf{I} \text{ N}^2 \cdot \text{m}^2$. In the simulations, $\boldsymbol{\tau} \in \{\tilde{\boldsymbol{\tau}}_b(\sigma), \tilde{\boldsymbol{\tau}}_\gamma(\sigma)\}$, with $\tilde{\boldsymbol{\tau}}_b(\sigma)$ defined as in [1] and

$$\tilde{\boldsymbol{\tau}}_\gamma(\sigma) = \mathbf{J} [k_\alpha \boldsymbol{\alpha}_e(\sigma) + k_\delta \dot{\boldsymbol{\alpha}}_e(\sigma) + k_\omega \boldsymbol{\omega}_e + \dot{\boldsymbol{\omega}}_d] + \boldsymbol{\omega} \times \mathbf{J} \boldsymbol{\omega}, \quad (20)$$

in which $\boldsymbol{\alpha}_e(\sigma) = \sigma \gamma(\Phi_e) \mathbf{u}_e$ and $\Phi_e = (1 - \sigma) \pi + \sigma \Theta_e$. Note that for $\sigma = +1$, $\Phi_e = \Theta_e$, and for $\sigma = -1$, $\Phi_e = 2\pi - \Theta_e$.

In total, we performed 10908 simulations of high-speed tumble-recovery maneuvers, in which the control objective was to stabilize the orientation of the UAV from an initial state with arbitrary attitude and angular velocity. Consistent with attitude regulation, for each simulation, the desired state was set to $\mathbf{q}_d = [1 \ 0 \ 0 \ 0]^T$ and $\boldsymbol{\omega}_d = \mathbf{0} \text{ rad} \cdot \text{s}^{-1}$. The directions of the initial Euler axes of rotation, $\mathbf{u}_0 = \mathbf{u}(t_0)$, were randomly selected from the unit sphere using a uniform distribution, and the initial rotations about \mathbf{u}_0 , $\Theta_0 = \Theta(t_0)$, were taken from the set $[1 : 180]^\circ$ in steps of 5° . For each Θ_0 , we varied the initial angular velocity, $\boldsymbol{\omega}_0$, from $-30 \cdot \mathbf{u}_0$ to $30 \cdot \mathbf{u}_0 \text{ rad} \cdot \text{s}^{-1}$ with the signed magnitude incremented in steps of $0.6 \text{ rad} \cdot \text{s}^{-1}$. For each simulated Θ_0 value, we computed the mean and *experimental standard deviation* (ESD) of the set of stabilization times, $\{t_s\}$ —with t_s defined as the time it takes for Θ_e to reach a value lower than 15° —corresponding to the set of 101 different simulated signed magnitudes of $\boldsymbol{\omega}_0$. Fig. 2(a) shows how the mean (solid line) and ESD (reduced-opacity band) of the stabilization time vary as functions of the initial rotation error, $\Theta_{e,0} = \Theta_e(t_0)$, for the three controllers. As seen, the means of the stabilization times obtained with the three controllers are similar for small values of $\Theta_{e,0}$; however, for larger values of $\Theta_{e,0}$, the means obtained with $\tilde{\boldsymbol{\tau}}_\gamma$ are notably smaller, even though τ_g produces a better performance in some cases—evidenced by the ESD data.

Fig. 2(b) shows the mean and ESD of the set of control efforts, $\{\Lambda\}$ —where $\Lambda = \int_0^1 \|\boldsymbol{\tau}(t)\|_2^2 dt$, for $\boldsymbol{\tau} \in \{\tilde{\boldsymbol{\tau}}_b, \tau_g, \tilde{\boldsymbol{\tau}}_\gamma\}$ —as functions of $\Theta_{e,0}$, for the same simulations corresponding to Fig. 2(a). Although the means of the control efforts obtained with the three controllers are similar for small values of $\Theta_{e,0}$, the values of Λ corresponding to $\tilde{\boldsymbol{\tau}}_b$ and $\tilde{\boldsymbol{\tau}}_\gamma$ decrease as $\Theta_{e,0}$ increases. Notably, the controller designed using the proposed method consistently requires less control effort while achieving a lower mean stabilization time compared to the two

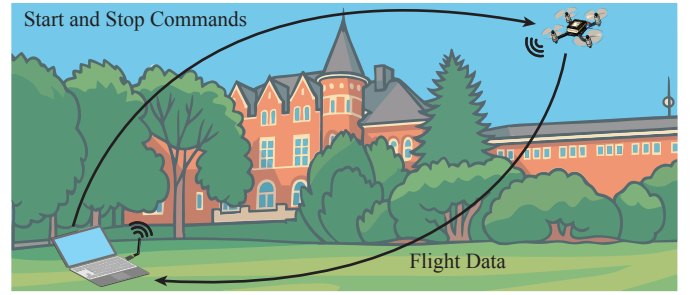


Fig. 3. Experimental setup used during the flight tests. The attitude control flight experiments were run outdoors using a ground computer equipped with the Crazyradio 2.0 to communicate with the Crazyflie 2.1.

benchmark controllers. Fig. 2(c) shows the time evolution of Θ_e corresponding to the three simulated control laws, with an initial condition of $\Theta_0 = 136^\circ$ and $\boldsymbol{\omega}_0 = 30 \cdot \mathbf{u}_0 \text{ rad} \cdot \text{s}^{-1}$. This initial state coincides with a kinematic condition in which the direction of the system’s initial angular velocity is opposite to that of the shorter rotational path required to eliminate the attitude error. As seen, the controller based on $\tilde{\boldsymbol{\tau}}_\gamma$ achieves a stabilization time of 0.45 s whereas the benchmark controllers—with laws $\tilde{\boldsymbol{\tau}}_b$ and τ_g —achieve stabilization times of 0.58 and 0.49 s, respectively. The initial rotation error, $\Theta_{e,0}$, for the $\tilde{\boldsymbol{\tau}}_b$ and $\tilde{\boldsymbol{\tau}}_\gamma$ cases is 224° , which means that these two laws applied the proportional component of the control torque in the direction of the longer rotational path required to eliminate the attitude error. Fig. 2(d) shows the corresponding SEA norms, $\|\mathbf{n}_e\|_2$ and $\|\boldsymbol{\alpha}_e\|_2$. As seen, $\|\mathbf{n}_e\|_2$ increases as the rotation error, Θ_e , decreases from 224° down to 180° and starts decreasing after passing through that point (see inset), which highlights the characteristic behavior of quaternion-based controllers. In contrast, $\|\boldsymbol{\alpha}_e\|_2$ increases and decreases with Θ_e , as intended by design.

B. Real-Time Flight Experiments

To further assess and demonstrate the suitability and performance of the proposed axis-angle control approach, we performed real-time flight experiments using the same three controllers described in Section IV-A. As depicted in Fig. 3, the flight tests were conducted outdoors, using a ground computer—equipped with the Crazyradio 2.0 2.4-GHz USB radio transceiver—to send initialization and stop commands, and collect the flight and control data at a rate of 100 Hz. During each test, the UAV was commanded to execute a high-speed tumble-recovery maneuver after a throw launch. A representative experiment consists of two stages. First, the tested UAV is thrown into the air with an unknown high angular velocity, while the controller and propellers remain inactive; then, the controller and propellers are activated. Throughout a maneuver, the flier operates entirely autonomously, using only onboard sensing and computation, with the tested attitude controller running at 500 Hz.

Fig. 4(a) presents the time evolution of Θ_e for three different experiments with similar initial conditions, using the three tested control laws. As seen, the stabilization times corresponding to $\tilde{\boldsymbol{\tau}}_b$, τ_g , and $\tilde{\boldsymbol{\tau}}_\gamma$ are 0.57, 0.50, and 0.48 s, respectively. Interestingly, the corresponding values of Λ for the τ_g and $\tilde{\boldsymbol{\tau}}_\gamma$ laws are 1.76×10^{-4} and $4.56 \times 10^{-5} \text{ N}^2 \cdot \text{m}^2 \cdot \text{s}$, which indicates that the proposed method achieved a lower stabilization

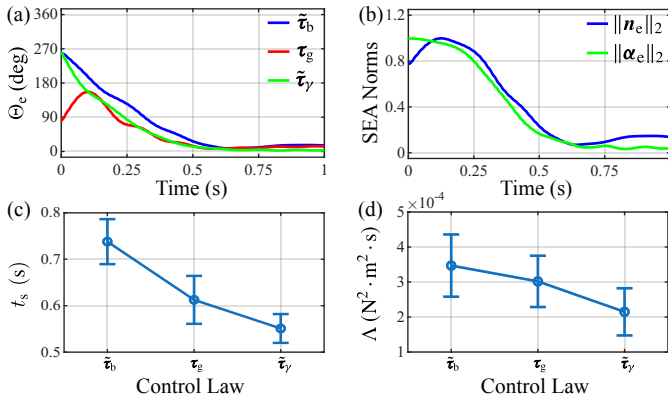


Fig. 4. Experimental flight results. (a) Rotation errors, as functions of time, corresponding to tests performed using $\tilde{\tau}_b$, τ_g , and $\tilde{\tau}_\gamma$. (b) Time evolutions of the SEA magnitudes, $\|n_e\|_2$ and $\|\alpha_e\|_2$, corresponding to the tests performed using $\tilde{\tau}_b$ and $\tilde{\tau}_\gamma$, respectively, shown in (a). (c) Comparison of the means (circles) and SEM values (vertical bars) of the stabilization times, corresponding to 30 independent tests per control law, for flights performed using $\tilde{\tau}_b$, τ_g , and $\tilde{\tau}_\gamma$. (d) Comparison of the means and SEM values of the control efforts corresponding to the same 30 tests per control law of the data shown in (c).

time using only about 25% of the control effort measured for the geometric-control case. Fig. 4(b) presents the time evolutions of the SEA norms $\|n_e\|_2$ and $\|\alpha_e\|_2$. Similarly to the simulation cases discussed in Section IV-A, it can be observed that $\|n_e\|_2$ increases as Θ_e decreases down to 180° from approximately 270°, and decreases after passing through this point. In contrast, over the entire range of operation, $\|\alpha_e\|_2$ decreases and increases with Θ_e , as intended by design. Experiments of this type can be viewed in the video available as a Supplemental Item.

In Fig. 4(c), each data point indicates the mean and *standard error of the mean* (SEM) of the stabilization times corresponding to 30 back-to-back experiments performed using each of the three control laws compared in this letter. The means of the stabilization times corresponding to $\tilde{\tau}_b$, τ_g , and $\tilde{\tau}_\gamma$ are 0.74, 0.61, and 0.55 s, respectively. In Fig. 4(d), each data point indicates the mean and SEM of the control efforts, Λ , corresponding to the same experiments of the data shown in Fig. 4(c). The means of the Λ values corresponding to $\tilde{\tau}_b$, τ_g , and $\tilde{\tau}_\gamma$ are 3.47×10^{-4} , 3.02×10^{-4} , and $2.15 \times 10^{-4} N^2 \cdot m^2 \cdot s$, respectively. Although the differences between these values are not substantial, the recorded experimental data provide compelling evidence of the suitability and superior performance of the proposed approach; particularly, under nonideal conditions due to the presence of actuator saturation, model uncertainty, and disturbances. We infer that these real-world conditions also explain the discrepancies between the simulated and experimental Λ values. The large variability in the experimental data is expected due to the random nature of tumble-recovery experiments.

V. CONCLUSION

We introduced a new class of axis-angle attitude control laws that provide substantial design flexibility with guaranteed CL stability while ensuring a greater proportional control effort the farther the system's state is from the unique stable fixed AEQ of the CL dynamics. This characteristic is particularly useful when the proposed approach is used in combination with intelligent switching schemes. Evidence regarding functionality and high performance was provided in the form of data obtained through

simulations and outdoor flight tests, during which we commanded a quadrotor to autonomously execute tumble-recovery maneuvers in the air. From a statistical standpoint, the new method consistently achieved reduced stabilization times and required less control effort compared to the quaternion-based and geometric-control methods used as benchmarks.

REFERENCES

- [1] F. M. F. R. Gonçalves, R. M. Bena, K. I. Matveev, and N. O. Pérez-Arancibia, "MPS: A new method for selecting the stable closed-loop equilibrium attitude-error quaternion of a UAV during flight," in *Proc. IEEE Int. Conf. Robot. Autom. (ICRA)*, Yokohama, Japan, May 2024, pp. 8363–8369.
- [2] F. M. F. R. Gonçalves, R. M. Bena, and N. O. Pérez-Arancibia, "Closed-loop stability of a Lyapunov-based switching scheme for energy-efficient torque-input-selection during flight," in *Proc. IEEE Int. Conf. Robot. Biomim. (ROBIO)*, Bangkok, Thailand, Dec. 2024, pp. 1941–1947.
- [3] R. Schlanbusch, A. Loria, and P. J. Nicklasson, "On the stability and stabilization of quaternion equilibria of rigid bodies," *Automatica*, vol. 48, no. 12, pp. 3135–3141, 2012.
- [4] R. M. Bena, X.-T. Nguyen, X. Yang, A. A. Calderón, Y. Chen, and N. O. Pérez-Arancibia, "A multiplatform position control scheme for flying robotic insects," *J. Intell. Robot. Syst.*, vol. 105, no. 1, May 2022, Art. no. 19.
- [5] R. M. Bena, X. Yang, A. A. Calderón, and N. O. Pérez-Arancibia, "High-performance six-DOF flight control of the Bee⁺⁺: An inclined-stroke-plane approach," *IEEE Trans. Robot.*, vol. 39, no. 2, pp. 1668–1684, Apr. 2023.
- [6] C. G. Mayhew, R. G. Sanfelice, and A. R. Teel, "Robust global asymptotic attitude stabilization of a rigid body by quaternion-based hybrid feedback," in *Proc. IEEE Conf. Decis. Control (CDC), Chin. Control Conf. (CCC)*, Shanghai, China, Dec. 2009, pp. 2522–2527.
- [7] —, "On quaternion-based attitude control and the unwinding phenomenon," in *Proc. Amer. Control Conf. (ACC)*, San Francisco, CA, USA, Jun. 2011, pp. 299–304.
- [8] —, "Quaternion-based hybrid control for robust global attitude tracking," *IEEE Trans. Autom. Control*, vol. 56, no. 11, pp. 2555–2566, Nov. 2011.
- [9] B. Pratama, A. Muis, A. Subiantoro, M. Djemai, and R. B. Atitallah, "Quadcopter trajectory tracking and attitude control based on Euler angle limitation," in *Proc. 6th Int. Conf. Control Eng. Inf. Technol. (CEIT)*, Istanbul, Turkey, Oct. 2018, Art. no. 8751819.
- [10] A. Mokhtari and A. Benallegue, "Dynamic feedback controller of Euler angles and wind parameters estimation for a quadrotor unmanned aerial vehicle," in *Proc. IEEE Int. Conf. Robot. Autom. (ICRA)*, New Orleans, LA, USA, Apr. 2004, pp. 2359–2366.
- [11] C. W. Kang and C. G. Park, "Euler angle based attitude estimation avoiding the singularity problem," in *Proc. 18th IFAC World Cong. (IFAC-WC)*, Milan, Italy, Aug. 2011, pp. 2096–2102.
- [12] T. Lee, "Geometric tracking control of the attitude dynamics of a rigid body on $SO(3)$," in *Proc. Amer. Control Conf. (ACC)*, San Francisco, CA, USA, Jun. 2011, pp. 1200–1205.
- [13] —, "Geometric control of quadrotor UAVs transporting a cable-suspended rigid body," *IEEE Trans. Control Syst. Technol.*, vol. 26, no. 1, pp. 255–264, Jan. 2018.
- [14] G. Wu and K. Sreenath, "Geometric control of multiple quadrotors transporting a rigid-body load," in *Proc. IEEE Conf. Decis. Control (CDC)*, Los Angeles, CA, USA, Dec. 2014, pp. 6141–6148.
- [15] J. Wei, S. Zhang, A. Adaldo, X. Hu, and K. H. Johansson, "Finite-time attitude synchronization with a discontinuous protocol," in *Proc. Int. Conf. Control Autom. (ICCA)*, Ohrid, Macedonia, Jul. 2017, pp. 192–197.
- [16] J. Thunberg, W. Song, E. Montijano, Y. Hong, and X. Hu, "Distributed attitude synchronization control of multi-agent systems with switching topologies," *Automatica*, vol. 50, no. 3, pp. 832–840, Mar. 2014.
- [17] N. A. Chaturvedi, A. K. Sanyal, and N. H. McClamroch, "Rigid-body attitude control," *IEEE Control Syst. Mag.*, vol. 31, no. 3, pp. 30–51, Jun. 2011.
- [18] J. B. Kuipers, *Quaternions and Rotation Sequences: A Primer with Applications to Orbits, Aerospace and Virtual Reality*. Princeton, NJ, USA: Princeton University Press, 2002.
- [19] A. D. Ames, X. Xu, J. W. Frizzle, and P. Tabuada, "Control barrier function based quadratic programs for safety critical systems," *IEEE Trans. Autom. Control*, vol. 62, no. 8, pp. 3861–3876, Aug. 2017.
- [20] O. Hájek, "Discontinuous differential equations, I," *J. Differ. Equ.*, vol. 32, no. 2, pp. 149–170, May 1979.